

TOWARDS SYMMETRY-UNRESTRICTED  
SKYRME–HFB IN COORDINATE-SPACE  
REPRESENTATION: THE EXAMPLE OF ROTATIONAL  
BANDS OF THE OCTUPOLE-DEFORMED  
NUCLEUS  $^{222}\text{Th}^*$

W. RYSENS, M. BENDER

IPNL, Université de Lyon, Université Lyon 1, CNRS/IN2P3  
69622 Villeurbanne, France

P.-H. HEENEN

PNTPM, CP229, Université Libre de Bruxelles, 1050 Bruxelles, Belgium

*(Received December 13, 2017)*

We report on the cranked Skyrme–HFB calculations of rotational bands of the octupole-deformed nucleus  $^{222}\text{Th}$ . A sudden change in configuration is observed, with the shape of the yrast state jumping from large octupole deformation at low spin to small octupole deformation at high spin.

DOI:10.5506/APhysPolB.49.339

## 1. Introduction

Applications of the self-consistent mean-field approach have a long-standing history in nuclear structure physics [1]. Starting from an energy density functional (EDF) that models the effective nucleon–nucleon interaction in the medium, this microscopic method provides versatile tools to study the structure of nuclei across the entire nuclear chart. Their applications are not limited to ground-state properties, but can be extended to excited configurations such as  $K$ -isomers and rotational bands.

Recently, we have set up a new code named MOCCa for such calculations [2] that is based on the time-tested principles of our previous ones [3–7], but unifies them into a single scheme with many new functionalities. As before, single-particle wave functions are represented on a 3d Cartesian Lagrange

---

\* Presented at the XXXV Mazurian Lakes Conference on Physics, Piaski, Poland, September 3–9, 2017.

mesh in coordinate space [7], and the Hartree–Fock–Bogoliubov (HFB) equations are solved with the two-basis methods [6]. The code’s most important new features concern the variational space, where the point-group symmetries [8] imposed in earlier codes can now be individually lifted.

As an example of the large range of physical situations to which the new code can be applied, we present results on rotational bands of  $^{222}\text{Th}$ . This nucleus has the particularity of having rotational bands of alternating parity that are connected by strong electric dipole transitions [9]. In a mean-field picture of the nucleus, such an experimental finding can be associated with a pear-shaped octupole-deformed ground-state configuration [10, 11]. The study of octupole deformations in this and other regions of the chart of nuclei is presently the subject of intense experimental activity [12–16].

The appearance of octupole-deformed minima in mean-field calculations of the deformation energy surface is limited to small regions of the nuclear chart around specific combinations of proton and neutron numbers [17, 18]. With  $Z = 90$ , some thorium isotopes fall into such a region: While reflection-symmetric mean-field minima are found for the lighter isotopes up to about  $^{218}\text{Th}$ , calculations for those around  $^{226}\text{Th}$  exhibit pronounced octupole-deformed minima, which again fade away when going to even heavier isotopes. The exact location of the transition between symmetric and asymmetric shapes depends, however, on details of the parameterisation of the EDF used for the calculations.

Nuclear shapes do not only change with  $N$  and  $Z$ , they also can change with angular momentum  $J$ . Macroscopic–microscopic models [19, 20] predict that the octupole deformation of the ground-state of  $^{222}\text{Th}$  does not persist to high  $J$ . Direct experimental evidence is still lacking, but the observed sudden drop in intensity of the populated states at high  $J$  could be the fingerprint of such a change in shape [9].

Rotational bands of octupole-deformed nuclei have been studied at high spin using the cranked HF [21] and HFB [22, 23] methods, but, to the best of our knowledge, an abrupt change at high  $J$ -value has not been put into evidence before.

## 2. Skyrme–HFB description of octupole deformed shapes

We will first address the description of the ground-state, postponing the discussion of rotational bands to the next section. We carry out self-consistent HFB calculations using the SLy5s1 parameterisation [24] of the Skyrme EDF in the particle–hole channel. This recent fit has been adjusted with a constraint on the surface energy coefficient  $a_{\text{surf}}$  and provides a very satisfying description of the deformation properties of heavy nuclei [25]. For the pairing channel, we add a surface-type contact interaction in conjunction with the Lipkin–Nogami procedure, with parameters as defined in Ref. [26].

As discussed above, both quadrupole and octupole correlations play a significant role for nuclei around  $^{222}\text{Th}$ . While non-axial degrees of freedom are accessible in our codes, it turns out that at intrinsic angular momentum zero, the lowest mean-field states retain axial symmetry. As a consequence, we can label single-particle states by the projection  $K$  of their angular momentum on the symmetry axis, and characterise nuclear shapes with the dimensionless multipole moments  $\beta_{20}$  and  $\beta_{30}$

$$\beta_{20} = \frac{4\pi}{3R_0^2 A} \sqrt{\frac{5}{16\pi}} \langle 2\hat{z}^2 - \hat{x}^2 - \hat{y}^2 \rangle, \quad (1)$$

$$\beta_{30} = \frac{4\pi}{3R_0^3 A} \sqrt{\frac{7}{16\pi}} \langle \hat{z} (2\hat{z}^2 - 3\hat{x}^2 - 3\hat{y}^2) \rangle, \quad (2)$$

where  $R_0 \equiv 1.2A^{1/3}$  fm and the  $z$ -axis is chosen as reference axis. Non-zero values for either indicate broken rotational symmetry in the mean-field state, non-zero values for  $\beta_{30}$  the additional breaking of parity. This is accompanied by the loss of parity and angular momentum quantum numbers for the many-body as well as the single-particle states. As the self-consistent minimisation leads to states for which the multipole moments  $\beta_{\ell m}$  are zero for all combinations of odd  $\ell$  with  $m \neq 0$ , we can, however, impose two spatial point-group symmetries on their calculation in a 3d code without influencing the result. These are  $z$ -signature  $\hat{R}_z$  and the  $y$ -time simplex  $\hat{S}_y^T$  as defined in [8]. In addition, for the ground state of this even-even nucleus, we can enforce time-reversal symmetry. These are the choices that have been made when setting up the Ev4 code for HF+BCS calculations used in [4].

Some results relevant for the analysis of the mean-field energy surface of  $^{222}\text{Th}$  can be found in Fig. 1. Panel (a) shows the deformation energy as a function of  $\beta_{20}$  and  $\beta_{30}$ . A pronounced minimum is visible at  $(\beta_{20}, \beta_{30}) \approx (0.15, 0.12)$ , which is about 1 MeV lower than the reflection-symmetric saddle point at  $(0.14, 0)$ . This finding differs from relativistic mean-field results obtained with the DD-PC1 and NL3 parameterisations [27, 28], where it is only for  $^{224}\text{Th}$  (DD-PC1) or even  $^{226}\text{Th}$  (NL3) that a minimum at comparable deformations appears, while  $^{222}\text{Th}$  remains spherical. In fact, in our calculations, static octupole deformation already sets in for  $^{220}\text{Th}$ , see panels (b1) and (b2) of Fig. 1. The same is found for the D1S parameterisation of the Gogny force [17], whereas for D1M octupole deformation sets in with  $^{222}\text{Th}$  [17]. On the experimental side, rotational alternating parity bands are observed beginning with  $^{222}\text{Th}$ , while the spectrum of  $^{220}\text{Th}$  requires a different interpretation [14].

The effect of deforming  $^{222}\text{Th}$  on its single-particle levels is shown in panels on the right. They display the Nilsson diagram of eigenvalues of the single-particle Hamiltonian for neutrons (c1) and protons (c2). For small

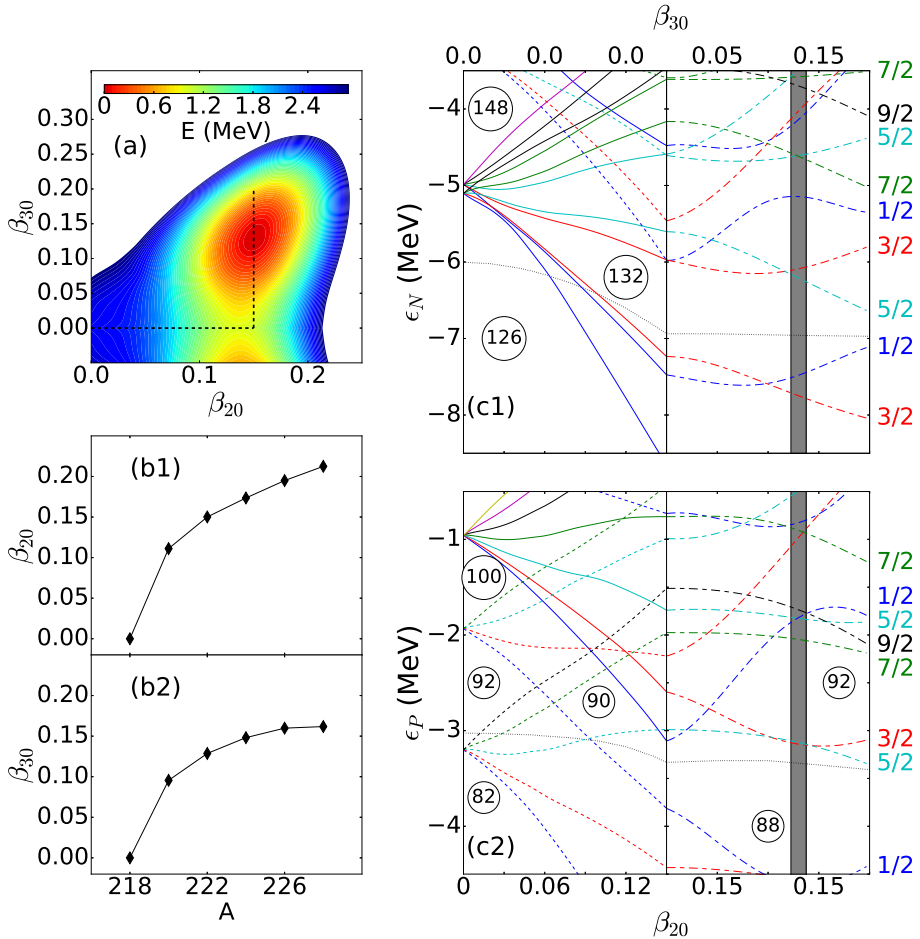


Fig. 1. (Colour on-line) Deformation energy of  $^{222}\text{Th}$  relative to the ground state in the  $\beta_{20}$ - $\beta_{30}$  plane (a); quadrupole (b1) and octupole deformation (b2) of the mean-field minimum of the thorium isotopes; Nilsson diagram of neutrons (c1) and protons (c2) along a path in deformation space (see the text) as indicated by the black/dashed line in panel (a). States are colour-coded according to their  $K$  quantum number. The grey band indicates the location of the overall minimum.

deformations up to the vertical line, these quantities are plotted as a function of quadrupole deformation  $\beta_{20}$ , keeping  $\beta_{30} = 0$ . Beyond the vertical line,  $\beta_{30}$  is varied, while  $\beta_{20}$  is kept constant at the value of the absolute minimum. Different colours indicate the levels'  $K$  quantum number as listed in the legend. For reflection-symmetric configurations,  $\beta_{30} = 0$ , solid and short-dashed lines represent levels of positive and negative parity, respectively.

When  $\beta_{30} \neq 0$ , parity is not a good single-particle quantum number and all levels are drawn with long-dashed lines. The Fermi energies of protons and neutrons are displayed with grey/dotted lines.

One can see that the quadrupole and octupole deformations collaborate to produce sizeable gaps in both the proton and neutron single-particle spectra for  $Z = 88$ ,  $N = 132$  at  $(\beta_{20}, \beta_{30}) \approx (0.15, 0.12)$ . While both gaps are also present in the spectra at the symmetric saddle point, the octupole deformation results in a further opening of the respective gap for both particle species. The presence of the same gaps for octupole-deformed nuclei has already been reported earlier in Refs. [11, 29].

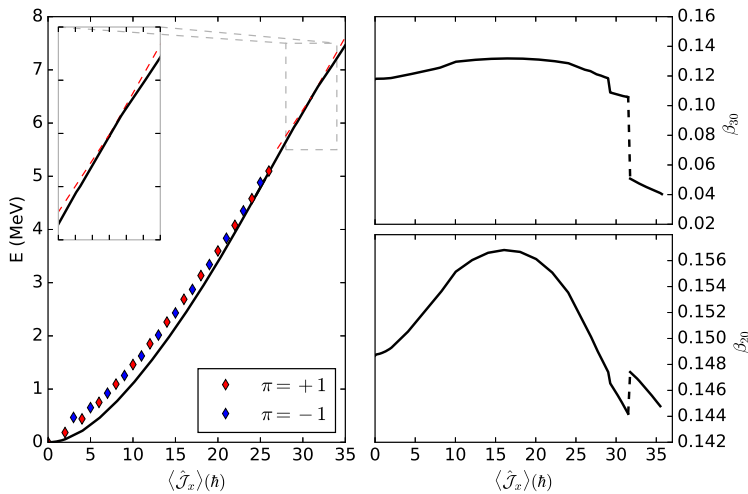


Fig. 2. (Colour on-line) Left: Excitation energy of rotational states of  $^{222}\text{Th}$  as a function of  $\langle \hat{J}_x \rangle$  as obtained in cranked HFB calculations (black/solid line) compared to the experimental data (diamond markers) for yrast states of positive (lighter/red) and negative (darker/blue) parity taken from [9]. The inset zooms on the transition region. Dashed lines are linear extrapolations of the curve before and after the transition and are only shown to guide the eye. The panels on the right display the calculated values of  $\beta_{30}$  (top) and  $\beta_{20}$  (bottom) along the band.

### 3. Cranked Skyrme–HFB for rotating octupole shapes

To describe rotational bands in a self-consistent mean-field approach, it is customary to vary the energy subject to a cranking constraint [5, 30]

$$R = E - \omega \cdot \langle \hat{\mathcal{J}} \rangle. \quad (3)$$

While our new code can handle arbitrary orientations of the many-body angular momentum vector  $\mathcal{J}$ , we will limit ourselves here to rotation about

a principal axis perpendicular to the symmetry axis of the ground state of  $^{222}\text{Th}$ , chosen to be the  $x$ -axis. The presence of the constraint in Eq. (3) requires one to lift several of the symmetries that could be imposed on calculations of that nucleus' ground state. First,  $\hat{\mathcal{J}}_x$  is a time-odd operator, such that time-reversal symmetry has to be abandoned. Second, finite values of  $\beta_{30}$  are only compatible with conserved  $z$  signature, while non-zero expectation values of  $\langle \hat{\mathcal{J}}_x \rangle$  are only compatible with  $x$  signature. Their combination rules out any conserved signature symmetry [8]. When pointing into a direction that is not a symmetry axis of the nucleus, finite values of  $\langle \hat{\mathcal{J}}_x \rangle$  are also incompatible with axial symmetry, such that the solution of the cranked HFB equations necessarily requires a 3d code as used here. From the symmetries mentioned in Sect. 2, only  $\hat{S}_y^T$  has been retained. All converged many-body states discussed here, however, conserve  $x$ -simplex  $\hat{S}_x$  as defined in [8], although it had not been imposed. The calculations can be carried out either for constant rotational frequency  $\omega_x$  or such that the solution takes a specific value for  $\langle \hat{\mathcal{J}}_x \rangle$ . Both have been used to construct states in the yrast band for which the energy, the quadrupole and the octupole deformations are shown in Fig. 2. At low spin, the behaviour of the energy is quadratical as it would be the case for a deformed classical rotor. At intermediate spins, deformations change slowly and the response of the energy to the cranking constraint becomes closer to linear. Between  $\langle \hat{\mathcal{J}}_x \rangle = 31$  and 32, however, the calculated energy shows a kink indicating an abrupt structural change in the system. At this point, all deformations exhibit a discontinuity. The change is very pronounced for the octupole deformation, decreasing from a large value  $\beta_{30} \approx 0.12$  to a much smaller one of  $\beta_{30} \approx 0.05$ . In comparison,  $\beta_{20}$  changes on a much smaller scale, which is a consequence of the rigidity of the potential energy surface in the quadrupole direction. A similar result has been obtained in a microscopic–macroscopic model [19, 20], but already at an angular momentum of about 24.

The calculated energies do not exhibit exactly the same behaviour as the available data. As cranked HFB is designed to describe high-spin states, some disagreement at low spin is not unexpected. It also has to be noted that pure cranked HFB can only calculate the energies of some mixture of states in the positive- and negative-parity bands of an octupole-deformed nucleus [22, 23]. As at all spins the energy surface is quite soft in octupole direction, any small change in the effective interaction might have a visible impact on the moment of inertia of this nucleus.

#### 4. Summary and outlook

We have studied the evolution of the shape of yrast states in the octupole deformed  $^{222}\text{Th}$  as a function of spin in cranked HFB calculations.

These calculations are technically challenging, as they require a 3d code in which the often imposed time-reversal, parity and signature symmetries are simultaneously lifted. The loss of the latter significantly complicates the numerical solution of the HFB equations [2].

Our calculations predict that yrast states undergo a sudden change from shapes with large octupole deformation to almost symmetric ones when spinning up the nucleus. Such transition has not been observed yet, but might occur for states at higher spins than those populated in past experiments [9]. New experimental data for the odd-mass neighbour  $^{223}\text{Th}$  point indeed towards such a shape change [16]. A detailed discussion of this system along the lines of the present study is in preparation.

The computations were performed using HPC resources from the computing centre of the IN2P3/CNRS and the Consortium des Équipements de Calcul Intensif (CÉCI), funded by the Fonds de la Recherche Scientifique de Belgique (F.R.S.-FNRS) under grant No. 2.5020.11. W.R. and P.-H.H. gratefully acknowledge funding by the IAP Belgian Science Policy (BriX network P7/12).

## REFERENCES

- [1] M. Bender *et al.*, *Rev. Mod. Phys.* **75**, 121 (2003).
- [2] W. Ryssens, Ph.D. Thesis, Université Libre de Bruxelles, 2016.
- [3] P. Bonche *et al.*, *Comp. Phys. Commun.* **171**, 49 (2005).
- [4] P. Bonche *et al.*, *Phys. Lett. B* **175**, 387 (1986).
- [5] P. Bonche *et al.*, *Nucl. Phys. A* **467**, 115 (1987).
- [6] B. Gall *et al.*, *Z. Phys. A* **348**, 183 (1994).
- [7] W. Ryssens *et al.*, *Comput. Phys. Commun.* **187**, 175 (2015).
- [8] J. Dobaczewski *et al.*, *Phys. Rev. C* **62**, 014310 (2000).
- [9] J.F. Smith *et al.*, *Phys. Rev. Lett.* **75**, 1050 (1995).
- [10] W. Nazarewicz *et al.*, *Nucl. Phys. A* **441**, 420 (1987).
- [11] P.A. Butler, W. Nazarewicz, *Rev. Mod. Phys.* **68**, 349 (1996).
- [12] L.P. Gaffney *et al.*, *Nature* **497**, 199 (2013).
- [13] P.A. Butler, *J. Phys. G* **43**, 073002 (2016).
- [14] W. Reviol *et al.*, *Phys. Rev. C* **90**, 044318 (2014).
- [15] B. Bucher *et al.*, *Phys. Rev. Lett.* **116**, 112503 (2016).
- [16] G. Maquart *et al.*, *Phys. Rev. C* **95**, 034304 (2017).
- [17] L.M. Robledo, G.F. Bertsch, *Phys. Rev. C* **84**, 054302 (2011).
- [18] S. Ebata, T. Nakatsukasa, *Phys. Scr.* **92**, 064005 (2017).

- [19] W. Nazarewicz *et al.*, *Phys. Rev. Lett.* **52**, 1272 (1984).
- [20] W. Nazarewicz *et al.*, *Nucl. Phys. A* **467**, 437 (1987).
- [21] A. Tsvetkov *et al.*, *J. Phys. G* **28**, 2187 (2002).
- [22] E. Garrote *et al.*, *Phys. Lett. B* **410**, 86 (1997).
- [23] E. Garrote *et al.*, *Phys. Rev. Lett.* **80**, 4398 (1998).
- [24] R. Jodon *et al.*, *Phys. Rev. C* **94**, 024335 (2016).
- [25] W. Ryssens *et al.*, in preparation.
- [26] C. Rigollet *et al.*, *Phys. Rev. C* **59**, 3120 (1999).
- [27] K. Nomura *et al.*, *Phys. Rev. C* **88**, 021303 (2013).
- [28] S.E. Agbemava *et al.*, *Phys. Rev. C* **93**, 044304 (2016).
- [29] J. Engel *et al.*, *Phys. Rev. C* **68**, 025501 (2003).
- [30] W. Satuła, R.A. Wyss, *Rep. Prog. Phys.* **68**, 131 (2005).